

Measurement of $\eta' \rightarrow \pi^+ \pi^- e^+ e^-$ and $\eta' \rightarrow \pi^+ \pi^- \mu^+ \mu^-$

M. Ablikim,¹ M. N. Achasov,⁶ O. Albayrak,³ D. J. Ambrose,³⁹ F. F. An,¹ Q. An,⁴⁰ J. Z. Bai,¹ R. Baldini Ferroli,^{17a} Y. Ban,²⁶ J. Becker,² J. V. Bennett,¹⁶ M. Bertani,^{17a} J. M. Bian,³⁸ E. Boger,^{19,*} O. Bondarenko,²⁰ I. Boyko,¹⁹ R. A. Briere,³ V. Bytev,¹⁹ H. Cai,⁴⁴ X. Cai,¹ O. Cakir,^{34a} A. Calcaterra,^{17a} G. F. Cao,¹ S. A. Cetin,^{34b} J. F. Chang,¹ G. Chelkov,^{19,*} G. Chen,¹ H. S. Chen,¹ J. C. Chen,¹ M. L. Chen,¹ S. J. Chen,²⁴ X. Chen,²⁶ Y. B. Chen,¹ H. P. Cheng,¹⁴ Y. P. Chu,¹ D. Cronin-Hennessy,³⁸ H. L. Dai,¹ J. P. Dai,¹ D. Dedovich,¹⁹ Z. Y. Deng,¹ A. Denig,¹⁸ I. Denysenko,^{19,†} M. Destefanis,^{43a,43c} W. M. Ding,²⁸ Y. Ding,²² L. Y. Dong,¹ M. Y. Dong,¹ S. X. Du,⁴⁶ J. Fang,¹ S. S. Fang,¹ L. Fava,^{43b,43c} C. Q. Feng,⁴⁰ P. Friedel,² C. D. Fu,¹ J. L. Fu,²⁴ O. Fuks,^{19,*} Y. Gao,³³ C. Geng,⁴⁰ K. Goetzen,⁷ W. X. Gong,¹ W. Gradl,¹⁸ M. Greco,^{43a,43c} M. H. Gu,¹ Y. T. Gu,⁹ Y. H. Guan,³⁶ A. Q. Guo,²⁵ L. B. Guo,²³ T. Guo,²³ Y. P. Guo,²⁵ Y. L. Han,¹ F. A. Harris,³⁷ K. L. He,¹ M. He,¹ Z. Y. He,²⁵ T. Held,² Y. K. Heng,¹ Z. L. Hou,¹ C. Hu,²³ H. M. Hu,¹ J. F. Hu,³⁵ T. Hu,¹ G. M. Huang,⁴ G. S. Huang,⁴⁰ J. S. Huang,¹² L. Huang,¹ X. T. Huang,²⁸ Y. Huang,²⁴ Y. P. Huang,¹ T. Hussain,⁴² C. S. Ji,⁴⁰ Q. Ji,¹ Q. P. Ji,²⁵ X. B. Ji,¹ X. L. Ji,¹ L. L. Jiang,¹ X. S. Jiang,¹ J. B. Jiao,²⁸ Z. Jiao,¹⁴ D. P. Jin,¹ S. Jin,¹ F. F. Jing,³³ N. Kalantar-Nayestanaki,²⁰ M. Kavatsyuk,²⁰ B. Kopf,² M. Kornicer,³⁷ W. Kuehn,³⁵ W. Lai,¹ J. S. Lange,³⁵ P. Larin,¹¹ M. Leyhe,² C. H. Li,¹ Cheng Li,⁴⁰ Cui Li,⁴⁰ D. M. Li,⁴⁶ F. Li,¹ G. Li,¹ H. B. Li,¹ J. C. Li,¹ K. Li,¹⁰ Lei Li,¹ Q. J. Li,¹ S. L. Li,¹ W. D. Li,¹ W. G. Li,¹ X. L. Li,²⁸ X. N. Li,¹ X. Q. Li,²⁵ X. R. Li,²⁷ Z. B. Li,³² H. Liang,⁴⁰ Y. F. Liang,³⁰ Y. T. Liang,³⁵ G. R. Liao,³³ X. T. Liao,¹ D. Lin,¹¹ B. J. Liu,¹ C. L. Liu,³ C. X. Liu,¹ F. H. Liu,²⁹ Fang Liu,¹ Feng Liu,⁴ H. Liu,¹ H. B. Liu,⁹ H. H. Liu,¹³ H. M. Liu,¹ H. W. Liu,¹ J. P. Liu,⁴⁴ K. Liu,³³ K. Y. Liu,²² Kai Liu,³⁶ P. L. Liu,²⁸ Q. Liu,³⁶ S. B. Liu,⁴⁰ X. Liu,²¹ Y. B. Liu,²⁵ Z. A. Liu,¹ Zhiqiang Liu,¹ Zhiqing Liu,¹ H. Loehner,²⁰ G. R. Lu,¹² H. J. Lu,¹⁴ J. G. Lu,¹ Q. W. Lu,²⁹ X. R. Lu,³⁶ Y. P. Lu,¹ C. L. Luo,²³ M. X. Luo,⁴⁵ T. Luo,³⁷ X. L. Luo,¹ M. Lv,¹ C. L. Ma,³⁶ F. C. Ma,²² H. L. Ma,¹ Q. M. Ma,¹ S. Ma,¹ T. Ma,¹ X. Y. Ma,¹ F. E. Maas,¹¹ M. Maggiora,^{43a,43c} Q. A. Malik,⁴² Y. J. Mao,²⁶ Z. P. Mao,¹ J. G. Messchendorp,²⁰ J. Min,¹ T. J. Min,¹ R. E. Mitchell,¹⁶ X. H. Mo,¹ H. Moeini,²⁰ C. Morales Morales,¹¹ K. Moriya,¹⁶ N. Yu. Muchnoi,⁶ H. Muramatsu,³⁹ Y. Nefedov,¹⁹ C. Nicholson,³⁶ I. B. Nikolaev,⁶ Z. Ning,¹ S. L. Olsen,²⁷ Q. Ouyang,¹ S. Pacetti,^{17b} J. W. Park,²⁷ M. Pelizaeus,² H. P. Peng,⁴⁰ K. Peters,⁷ J. L. Ping,²³ R. G. Ping,¹ R. Poling,³⁸ E. Prencipe,¹⁸ M. Qi,²⁴ S. Qian,¹ C. F. Qiao,³⁶ L. Q. Qin,²⁸ X. S. Qin,¹ Y. Qin,²⁶ Z. H. Qin,¹ J. F. Qiu,¹ K. H. Rashid,⁴² G. Rong,¹ X. D. Ruan,⁹ A. Sarantsev,^{19,‡} B. D. Schaefer,¹⁶ M. Shao,⁴⁰ C. P. Shen,^{37,§} X. Y. Shen,¹ H. Y. Sheng,¹ M. R. Shepherd,¹⁶ W. M. Song,¹ X. Y. Song,¹ S. Spataro,^{43a,43c} B. Spruck,³⁵ D. H. Sun,¹ G. X. Sun,¹ J. F. Sun,¹² S. S. Sun,¹ Y. J. Sun,⁴⁰ Y. Z. Sun,¹ Z. J. Sun,¹ Z. T. Sun,⁴⁰ C. J. Tang,³⁰ X. Tang,¹ I. Tapan,^{34c} E. H. Thorndike,³⁹ D. Toth,³⁸ M. Ullrich,³⁵ I. Uman,^{34b} G. S. Varner,³⁷ B. Q. Wang,²⁶ D. Wang,²⁶ D. Y. Wang,²⁶ K. Wang,¹ L. L. Wang,¹ L. S. Wang,¹ M. Wang,²⁸ P. Wang,¹ P. L. Wang,¹ Q. J. Wang,¹ S. G. Wang,²⁶ X. F. Wang,³³ X. L. Wang,⁴⁰ Y. D. Wang,^{17a} Y. F. Wang,¹ Y. Q. Wang,¹⁸ Z. Wang,¹ Z. G. Wang,¹ Z. Y. Wang,¹ D. H. Wei,⁸ J. B. Wei,²⁶ P. Weidenkaff,¹⁸ Q. G. Wen,⁴⁰ S. P. Wen,¹ M. Werner,³⁵ U. Wiedner,² L. H. Wu,¹ N. Wu,¹ S. X. Wu,⁴⁰ W. Wu,²⁵ Z. Wu,¹ L. G. Xia,³³ Y. X. Xia,¹⁵ Z. J. Xiao,²³ Y. G. Xie,¹ Q. L. Xiu,¹ G. F. Xu,¹ G. M. Xu,²⁶ Q. J. Xu,¹⁰ Q. N. Xu,³⁶ X. P. Xu,³¹ Z. R. Xu,⁴⁰ F. Xue,⁴ Z. Xue,¹ L. Yan,⁴⁰ W. B. Yan,⁴⁰ Y. H. Yan,¹⁵ H. X. Yang,¹ Y. Yang,⁴ Y. X. Yang,⁸ H. Ye,¹ M. Ye,¹ M. H. Ye,⁵ B. X. Yu,¹ C. X. Yu,²⁵ H. W. Yu,²⁶ J. S. Yu,²¹ S. P. Yu,²⁸ C. Z. Yuan,¹ Y. Yuan,¹ A. A. Zafar,⁴² A. Zallo,^{17a} S. L. Zang,²⁴ Y. Zeng,¹⁵ B. X. Zhang,¹ B. Y. Zhang,¹ C. Zhang,²⁴ C. C. Zhang,¹ D. H. Zhang,¹ H. H. Zhang,³² H. Y. Zhang,¹ J. Q. Zhang,¹ J. W. Zhang,¹ J. Y. Zhang,¹ J. Z. Zhang,¹ LiLi Zhang,¹⁵ R. Zhang,³⁶ S. H. Zhang,¹ X. J. Zhang,¹ X. Y. Zhang,²⁸ Y. Zhang,¹ Y. H. Zhang,¹ Z. P. Zhang,⁴⁰ Z. Y. Zhang,⁴⁴ Zhenghao Zhang,⁴ G. Zhao,¹ H. S. Zhao,¹ J. W. Zhao,¹ K. X. Zhao,²³ Lei Zhao,⁴⁰ Ling Zhao,¹ M. G. Zhao,²⁵ Q. Zhao,¹ S. J. Zhao,⁴⁶ T. C. Zhao,¹ X. H. Zhao,²⁴ Y. B. Zhao,¹ Z. G. Zhao,⁴⁰ A. Zhemchugov,^{19,*} B. Zheng,⁴¹ J. P. Zheng,¹ Y. H. Zheng,³⁶ B. Zhong,²³ L. Zhou,¹ X. Zhou,⁴⁴ X. K. Zhou,³⁶ X. R. Zhou,⁴⁰ C. Zhu,¹ K. Zhu,¹ K. J. Zhu,¹ S. H. Zhu,¹ X. L. Zhu,³³ Y. C. Zhu,⁴⁰ Y. M. Zhu,²⁵ Y. S. Zhu,¹ Z. A. Zhu,¹ J. Zhuang,¹ B. S. Zou,¹ and J. H. Zou¹

(BESIII Collaboration)

¹*Institute of High Energy Physics, Beijing 100049, People's Republic of China*²*Bochum Ruhr-University, D-44780 Bochum, Germany*³*Carnegie Mellon University, Pittsburgh, Pennsylvania 15213, USA*⁴*Central China Normal University, Wuhan 430079, People's Republic of China*⁵*China Center of Advanced Science and Technology, Beijing 100190, People's Republic of China*⁶*G. I. Budker Institute of Nuclear Physics SB RAS (BINP), Novosibirsk 630090, Russia*⁷*GSI Helmholtzcentre for Heavy Ion Research GmbH, D-64291 Darmstadt, Germany*⁸*Guangxi Normal University, Guilin 541004, People's Republic of China*⁹*GuangXi University, Nanning 530004, People's Republic of China*

- ¹⁰Hangzhou Normal University, Hangzhou 310036, People's Republic of China
¹¹Helmholtz Institute Mainz, Johann-Joachim-Becher-Weg 45, Mainz D-55099, Germany
¹²Henan Normal University, Xinxiang 453007, People's Republic of China
¹³Henan University of Science and Technology, Luoyang 471003, People's Republic of China
¹⁴Huangshan College, Huangshan 245000, People's Republic of China
¹⁵Hunan University, Changsha 410082, People's Republic of China
¹⁶Indiana University, Bloomington, Indiana 47405, USA
^{17a}INFN Laboratori Nazionali di Frascati, Frascati I-00044, Italy
^{17b}INFN and University of Perugia, Perugia I-06100, Italy
¹⁸Johannes Gutenberg University of Mainz, Johann-Joachim-Becher-Weg 45, Mainz D-55099, Germany
¹⁹Joint Institute for Nuclear Research, Dubna 141980, Moscow region, Russia
²⁰KVI, University of Groningen, NL-9747 AA Groningen, The Netherlands
²¹Lanzhou University, Lanzhou 730000, People's Republic of China
²²Liaoning University, Shenyang 110036, People's Republic of China
²³Nanjing Normal University, Nanjing 210023, People's Republic of China
²⁴Nanjing University, Nanjing 210093, People's Republic of China
²⁵Nankai University, Tianjin 300071, People's Republic of China
²⁶Peking University, Beijing 100871, People's Republic of China
²⁷Seoul National University, Seoul 151-747, Korea
²⁸Shandong University, Jinan 250100, People's Republic of China
²⁹Shanxi University, Taiyuan 030006, People's Republic of China
³⁰Sichuan University, Chengdu 610064, People's Republic of China
³¹Soochow University, Suzhou 215006, People's Republic of China
³²Sun Yat-Sen University, Guangzhou 510275, People's Republic of China
³³Tsinghua University, Beijing 100084, People's Republic of China
^{34a}Ankara University, Dogol Caddesi, Tandogan 06100, Ankara, Turkey
^{34b}Dogus University, Istanbul 34722, Turkey
^{34c}Uludag University, Bursa 16059, Turkey
³⁵Universitaet Giessen, Giessen D-35392, Germany
³⁶University of Chinese Academy of Sciences, Beijing 100049, People's Republic of China
³⁷University of Hawaii, Honolulu, Hawaii 96822, USA
³⁸University of Minnesota, Minneapolis, Minnesota 55455, USA
³⁹University of Rochester, Rochester, New York 14627, USA
⁴⁰University of Science and Technology of China, Hefei 230026, People's Republic of China
⁴¹University of South China, Hengyang 421001, People's Republic of China
⁴²University of the Punjab, Lahore 54590, Pakistan
^{43a}University of Turin, Turin I-10125, Italy
^{43b}University of Eastern Piedmont, Alessandria I-15121, Italy
^{43c}INFN, Turin I-10125, Italy
⁴⁴Wuhan University, Wuhan 430072, People's Republic of China
⁴⁵Zhejiang University, Hangzhou 310027, People's Republic of China
⁴⁶Zhengzhou University, Zhengzhou 450001, People's Republic of China

(Received 29 March 2013; published 28 May 2013)

Based on a sample of 225.3 million J/ψ events accumulated with the BESIII detector at the BEPCII, the decays of $\eta' \rightarrow \pi^+ \pi^- l^+ l^-$ are studied via $J/\psi \rightarrow \gamma \eta'$. A clear η' signal is observed in the $\pi^+ \pi^- e^+ e^-$ mass spectrum, and the branching fraction is measured to be $\mathcal{B}(\eta' \rightarrow \pi^+ \pi^- e^+ e^-) = (2.11 \pm 0.12(\text{stat}) \pm 0.14(\text{syst})) \times 10^{-3}$, which is in good agreement with theoretical predictions and the previous measurement, but is determined with much higher precision. No η' signal is found in the $\pi^+ \pi^- \mu^+ \mu^-$ mass spectrum, and the upper limit is determined to be $\mathcal{B}(\eta' \rightarrow \pi^+ \pi^- \mu^+ \mu^-) < 2.9 \times 10^{-5}$ at the 90% confidence level.

DOI: [10.1103/PhysRevD.87.092011](https://doi.org/10.1103/PhysRevD.87.092011)

PACS numbers: 25.75.Gz, 14.40.Df, 12.38.Mh

* Also at the Moscow Institute of Physics and Technology, Moscow 141700, Russia.

† On leave from the Bogolyubov Institute for Theoretical Physics, Kiev 03680, Ukraine.

‡ Also at the PNPI, Gatchina 188300, Russia.

§ Present address: Nagoya University, Nagoya 464-8601, Japan.

I. INTRODUCTION

Since the η' was discovered in 1964 [1,2], there has been considerable interest in its decay both theoretically and experimentally because of its special role in low energy scale quantum chromodynamics theory. Its main decay

modes, including hadronic and radiative decays, have been well measured [3], but the study of η' anomalous decays is still an open field.

Recently, using the radiative decay $J/\psi \rightarrow \gamma \eta'$ via $\psi(3686) \rightarrow \pi^+ \pi^- J/\psi$ as the source of η' mesons, CLEO [4] reported the first observation of the conversion decay $\eta' \rightarrow \pi^+ \pi^- e^+ e^-$, which has been discussed for many years based on the vector meson dominance (VMD) model and chiral perturbation theory [5–7]. Theoretically this decay is expected to proceed via a virtual photon intermediate state, $\eta' \rightarrow \pi^+ \pi^- \gamma^* \rightarrow \pi^+ \pi^- e^+ e^-$, and provides a more stringent test of the theories since it involves off-shell photons. In accordance with theoretical predictions, the two prominent features expected for this decay are a peak with a long tail just above $2m_e$ in the $e^+ e^-$ ($M_{e^+ e^-}$) mass spectrum, and a dominant ρ^0 contribution in $M_{\pi^+ \pi^-}$. CLEO with limited statistics was unable to explore these distributions, although their measured branching fraction, $\mathcal{B}(\eta' \rightarrow \pi^+ \pi^- e^+ e^-) = (2.5_{-0.9}^{+1.2} \pm 0.5) \times 10^{-3}$ [4], was consistent with predicted values around 2×10^{-3} [5–7]. In addition, the search for $\eta' \rightarrow \pi^+ \pi^- \mu^+ \mu^-$, which is predicted to be lower by two orders of magnitude, was also performed. No evident signal was observed, and the upper limit, $\mathcal{B}(\eta' \rightarrow \pi^+ \pi^- \mu^+ \mu^-) < 2.4 \times 10^{-4}$, at the 90% confidence level (C.L.), was determined.

At BESIII a sample of $(225.3 \pm 2.8) \times 10^6$ [8] J/ψ events, corresponding to 1.2×10^6 η' events produced through the radiative decay $J/\psi \rightarrow \gamma \eta'$ [3], was collected in 2009, and offers a unique opportunity to study η' decays. In addition to $\eta' \rightarrow \pi^+ \pi^- l^+ l^-$, $\eta' \rightarrow \gamma \pi^+ \pi^-$ is also studied in order to determine the ratio of $\mathcal{B}(\eta' \rightarrow \pi^+ \pi^- l^+ l^-)$ to $\mathcal{B}(\eta' \rightarrow \gamma \pi^+ \pi^-)$. The advantage of measuring $\frac{\mathcal{B}(\eta' \rightarrow \pi^+ \pi^- l^+ l^-)}{\mathcal{B}(\eta' \rightarrow \gamma \pi^+ \pi^-)}$ is that uncertainties due to the number of J/ψ events, tracking efficiency from π^\pm and the radiative photon detection efficiency cancel.

II. THE EXPERIMENT AND MONTE CARLO SIMULATION

BEPCII is a double-ring $e^+ e^-$ collider designed for a peak luminosity of $10^{33} \text{ cm}^{-2} \text{ s}^{-1}$ at the center of mass energy of 3770 MeV. The cylindrical core of the BESIII detector consists of a helium-gas-based drift chamber (MDC) for charged track and particle identification (PID) by dE/dx , a plastic scintillator time-of-flight system, and a 6240-crystal CsI(Tl) Electromagnetic Calorimeter (EMC) for electron identification and photon detection. These components are all enclosed in a superconducting solenoidal magnet providing a 1.0-T magnetic field. The solenoid is supported by an octagonal flux-return yoke with resistive-plate-counter muon detector modules (MU) interleaved with steel. The geometrical acceptance for charged tracks and photons is 93% of 4π , and the resolutions for charged track momentum and photon energy at 1 GeV are

0.5% and 2.5%, respectively. More details on the features and capabilities of BESIII are provided in Ref. [9].

The estimation of backgrounds and the determinations of detection efficiencies are performed through Monte Carlo (MC) simulations. The BESIII detector is modeled with the GEANT4 [10,11]. The production of the J/ψ resonance is implemented with MC event generator KKMC [12,13], while the decays are performed with EVTGEN [14,15]. The possible hadronic backgrounds are studied using a sample of J/ψ inclusive events in which the known decays of the J/ψ are modeled with branching fractions being set to the world average values in PDG [3], while the unknown decays are generated with the LUNDCHARM model [16]. For $\eta' \rightarrow \pi^+ \pi^- l^+ l^-$ decays, a model [17] based on theoretical calculations using the vector meson dominant model with infinite-width corrections and pseudoscalar meson mixing [7] was developed.

III. ANALYSIS

A. $\eta' \rightarrow \pi^+ \pi^- l^+ l^-$

The final state in this analysis is $\gamma \pi^+ \pi^- l^+ l^-$, with l being an electron or a muon. The charged tracks in the polar angle range $|\cos \theta| < 0.93$ are reconstructed from hits in the MDC. Good charged tracks are required to pass within ± 10 cm of the interaction point in the beam direction and ± 1 cm in the plane perpendicular to the beam. Photon candidates are reconstructed by clustering the EMC crystal energies. The minimum energy is 25 MeV for barrel showers ($|\cos \theta| < 0.8$) and 50 MeV for end-cap showers ($0.86 < |\cos \theta| < 0.92$). To eliminate the showers from charged particles, a photon must be separated by at least 15° from any good charged track. An EMC timing requirement is used to suppress noise and energy deposits unrelated to the event. Candidate events are required to contain exactly four good charged tracks with zero net charge and at least one good photon. To determine the species of the final state particles and select the best photon when additional photons are found in an event, the combination with the minimum value of $\chi^2_{\gamma \pi^+ \pi^- l^+ l^-}$ is retained. Here $\chi^2_{\gamma \pi^+ \pi^- l^+ l^-} = \chi^2_{4C} + \sum_{j=1}^4 \chi^2_{\text{PID}}(j)$ is the sum of the chi-square from the four-constraint (4C) kinematic fit imposing energy and momentum conservation, and that from PID, formed by combining time-of-flight system and dE/dx information of each charged track for each particle hypothesis (pion, electron, or muon). Events with $\chi^2_{4C} < 75$ are kept as $\gamma \pi^+ \pi^- l^+ l^-$ candidates. A 4C kinematic fit under the hypothesis of $\gamma 2(\pi^+ \pi^-)$ is also performed, and $\chi^2_{\gamma 2(\pi^+ \pi^-)} > \chi^2_{\gamma \pi^+ \pi^- l^+ l^-}$ is required to reject possible background events from $J/\psi \rightarrow \gamma 2(\pi^+ \pi^-)$.

A very clear η' signal is observed in the $\pi^+ \pi^- e^+ e^-$ invariant mass distribution, shown in Fig. 1(a) after the above event selection. MC study shows that the dominant background events come from $J/\psi \rightarrow \gamma \eta'$, $\eta' \rightarrow \gamma \pi^+ \pi^-$ with the η' photon subsequently converted into an

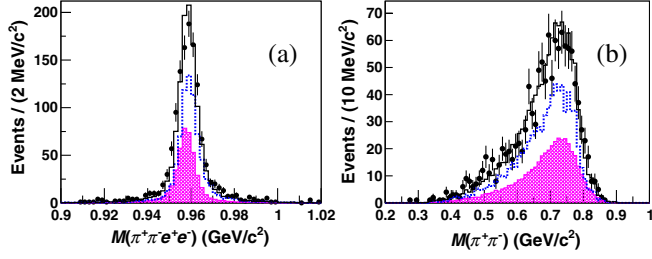


FIG. 1 (color online). Kinematical distributions for the η' to $\pi^+\pi^-e^+e^-$ decay: The invariant mass distributions of (a) $\pi^+\pi^-e^+e^-$ and (b) $\pi^+\pi^-$. Dots with error bars represent the data; the shaded area is MC signal shape, the dashed histogram is the $\eta' \rightarrow \gamma\rho^0(\pi^+\pi^-)$ MC line shape, and the solid histogram is the sum of MC signal and MC background from $\eta' \rightarrow \gamma\rho^0(\pi^+\pi^-)$. Both of these MC simulations are normalized to the yields found in Table I.

electron-positron pair; this background is displayed as the dashed histogram in Fig. 1(a). The di-pion invariant mass distribution, which is shown in Fig. 1(b), shows good agreement between data and MC simulation. Figure 2 displays the e^+e^- mass spectrum after requiring $|M(\pi^+\pi^-e^+e^-) - m(\eta')| < 0.02 \text{ GeV}/c^2$; the background from $\gamma\pi^+\pi^-$ conversions can be easily distinguished. The enhancement close to e^+e^- mass threshold corresponds to the signal from the $\eta' \rightarrow \pi^+\pi^-e^+e^-$ decay, and the clear peak around $0.015 \text{ GeV}/c^2$ comes from the background events of $\eta' \rightarrow \gamma\pi^+\pi^-$ where the photon undergoes conversion to an e^+e^- pair and the electron (positron)'s momentum is improperly reconstructed assuming that all the charged tracks are from the interaction point. The background contributions of $J/\psi \rightarrow \pi^+\pi^-\pi^0$ and $J/\psi \rightarrow \gamma\pi^+\pi^-\pi^0$ are estimated from the η' sideband region ($0.88 \text{ GeV}/c^2 < M(\pi^+\pi^-e^+e^-) < 0.90 \text{ GeV}/c^2$ or $1.02 \text{ GeV}/c^2 < M(\pi^+\pi^-e^+e^-) < 1.04 \text{ GeV}/c^2$).

To extract the $\eta' \rightarrow \pi^+\pi^-e^+e^-$ events, an unbinned extended maximum likelihood fit is performed on the

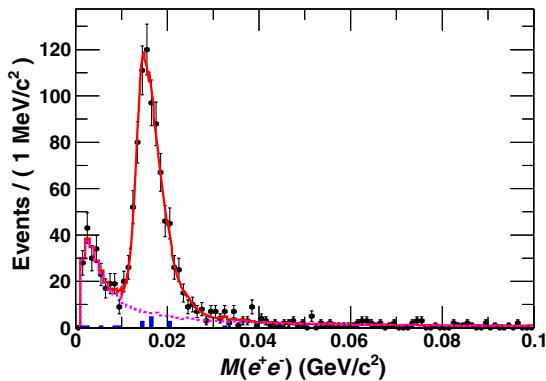


FIG. 2 (color online). The e^+e^- invariant mass spectrum of data (dots with error bars) after all selection criteria are applied. The solid line represents the fit result, the dotted histogram is the MC signal shape and the shaded histogram is background obtained from η' sideband events.

TABLE I. Numbers used in the branching fraction calculations: the fitted signal yields, N (or 90% C.L. upper limit); the detection efficiency, ϵ .

η' decay mode	ϵ (%)	N
$\pi^+\pi^-e^+e^-$	16.94 ± 0.08	429 ± 24
$\pi^+\pi^-\mu^+\mu^-$	35.47 ± 0.11	< 12
$\gamma\rho^0(\pi^+\pi^-)$	45.39 ± 0.07	158916 ± 425

observed e^+e^- invariant mass distribution with the signal shape described by the MC generator specifically developed for this analysis, the dominant background shape represented with the smoothed MC shape of $\eta' \rightarrow \gamma\pi^+\pi^-$, and the contribution (17 events) obtained from η' sideband fixed in the fit to account for the non- η' background. The fit, shown in Fig. 2, yields 429 ± 24 $\pi^+\pi^-e^+e^-$ events, and the detection efficiency obtained from MC simulation is $(16.94 \pm 0.08)\%$; both are summarized in Table I.

Figure 3 shows the $\pi^+\pi^-\mu^+\mu^-$ invariant mass spectrum for candidates surviving all selection criteria. The contribution from background events, mainly coming from $J/\psi \rightarrow \pi^0\pi^+\pi^-\pi^+\pi^-$ and $J/\psi \rightarrow \gamma\pi^+\pi^-\pi^+\pi^-$ and estimated with the inclusive MC J/ψ events, is shown as the dashed histogram. Although a few events accumulate in the η' mass region, they are not significant.

To determine the upper limit on the η' signal, a series of unbinned extended maximum likelihood fits is performed to the mass spectrum of $\pi^+\pi^-\mu^+\mu^-$ with an expected η' signal. In the fit, the line shape of the η' signal is determined by MC simulation, and the background is represented with a second-order Chebychev polynomial. The likelihood distributions of the fit are taken as the probability density function directly. The upper limit on the number of signal events at the 90% C.L. is defined as N^{UL} ,

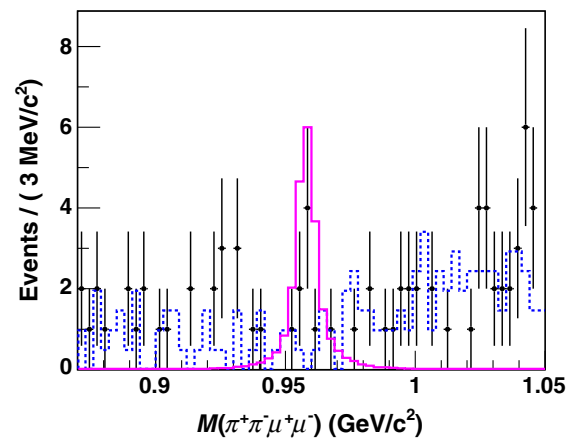
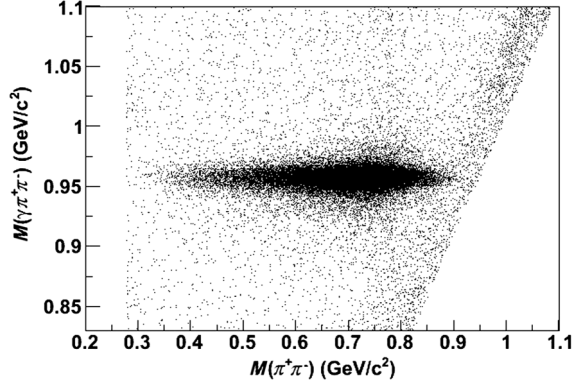


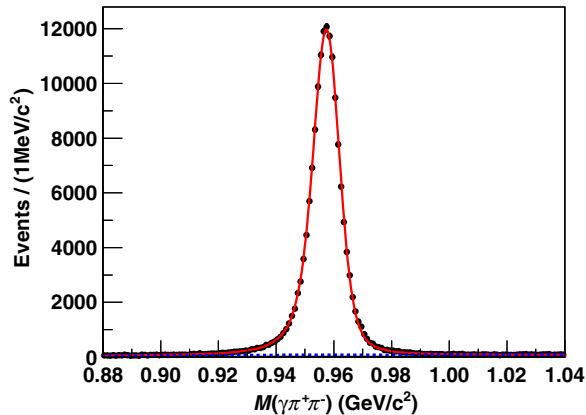
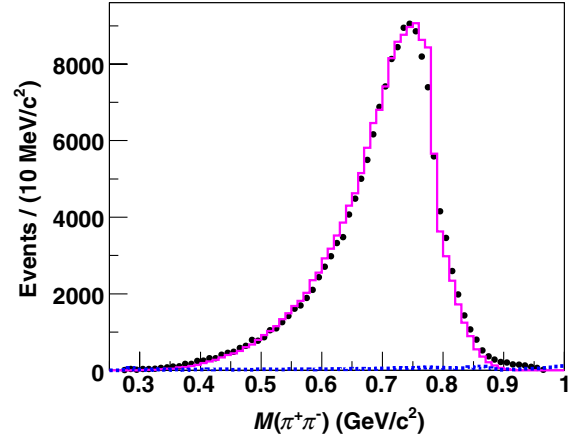
FIG. 3 (color online). The $\pi^+\pi^-\mu^+\mu^-$ invariant mass distributions of data and MC simulation with all selection criteria applied. Dots with error bars represent the data, the solid histogram is MC signal, and the dashed line indicates inclusive MC.

FIG. 4. Scatter plot of $M(\gamma\pi^+\pi^-)$ versus $M(\pi^+\pi^-)$ for data.

corresponding to the number of events at 90% of the integral of the probability density function. The fit-related uncertainties on N^{UL} are estimated by using different fit ranges and different orders of the background polynomial. The maximum one, $N^{\text{UL}} = 12$, and the detection efficiency from MC simulation, $(35.47 \pm 0.11)\%$, are used to evaluate the upper limit on the branching fraction.

B. $J/\psi \rightarrow \gamma\eta'$, $\eta' \rightarrow \gamma\pi^+\pi^-$

The final state is $\gamma\gamma\pi^+\pi^-$ for this mode. The charged track and good photon selection are the same as those described above, but no PID is applied in the event selection. A 4C kinematic fit is performed under the hypothesis of $J/\psi \rightarrow \pi^+\pi^-\gamma\gamma$, and $\chi_{4C}^2 < 75$ is required. For events with more than two photon candidates, the combination with the minimum χ_{4C}^2 is retained. To reject background events with π^0 in the final state, the invariant mass of the two photons is required to satisfy $M(\gamma\gamma) > 0.16 \text{ GeV}/c^2$; this removes 94% background while the efficiency loss is only 0.73%. The experimental signature of $J/\psi \rightarrow \gamma\eta'$ ($\eta' \rightarrow \gamma\pi^+\pi^-$) is given by the radiative photon from J/ψ

FIG. 5 (color online). The $\gamma\pi^+\pi^-$ invariant mass spectrum for data after all selection criteria are applied. The solid curve is the fit result, and the dashed line represents the background polynomial.FIG. 6 (color online). The comparison of the simulated $\pi^+\pi^-$ mass spectrum with data. Dots with error bars are data within the η' region ($[0.938, 0.978] \text{ GeV}/c^2$), the dashed histogram is background obtained from the η' sideband, and the solid histogram represents the MC simulation.

decays, that carries a unique energy of 1.4 GeV. Consequently it is easy to distinguish this photon from those from η' decays. In this analysis, the combination of $\gamma\pi^+\pi^-$ invariant mass closest to the η' mass is chosen to reconstruct the η' .

Figure 4 shows the scatter plot of $M(\gamma\pi^+\pi^-)$ versus $M(\pi^+\pi^-)$ for the candidate events, where the distinct $\eta' - \rho^0$ band corresponds to the decay $\eta' \rightarrow \gamma\pi^+\pi^-$. A very clean η' peak is observed in the $M(\gamma\pi^+\pi^-)$ distribution, as displayed in Fig. 5. The peak is fitted with the MC simulated signal shape convolved with a Gaussian mass resolution function to account for the difference in mass resolution between data and MC simulations, plus a second-order Chebychev polynomial background shape. The fit, shown as the smooth curve in Fig. 5 gives 158916 ± 425 $\eta' \rightarrow \gamma\pi^+\pi^-$ events, and the detection efficiency, $(45.39 \pm 0.07)\%$, is obtained from the MC simulation; these are tabulated in Table I. In the simulation of $\eta' \rightarrow \gamma\pi^+\pi^-$, since the resonant contribution from $\rho^0 \rightarrow \pi^+\pi^-$ is insufficient to describe the data, the non-resonant contribution (known as the ‘‘box anomaly’’) is also included using a decay rate formula [18] deduced from the ones used in Refs. [20–22]. With the parameters tuned with data, the comparison of the simulated dipion mass spectrum to data in Fig. 6 shows good agreement.

IV. SYSTEMATIC ERRORS

In the measurement of the ratio of the branching fractions, the possible systematic error sources and the corresponding contributions are discussed in detail below.

- (i) Form factor uncertainty. In the MC generator used to determine the detection efficiency of $\eta' \rightarrow \pi^+\pi^-l^+l^-$, the VMD factor defined for the hidden gauge model is introduced to account for the contribution from the ρ^0 meson. The detection

efficiency dependence is evaluated by replacing the factor above with the modified VMD factors denoted in Ref. [7]. The maximum change of the detection efficiencies is assigned as the systematic error, which is listed in Table II.

- (ii) MDC tracking efficiency. Due to the similar dynamics of $\eta' \rightarrow \pi^+ \pi^- \gamma^* \rightarrow \pi^+ \pi^- l^+ l^-$ and $\eta' \rightarrow \gamma \pi^+ \pi^-$, the systematic errors for the two charged pions cancel in the calculation of the relative branching fraction of $\eta' \rightarrow \pi^+ \pi^- l^+ l^-$ and $\eta' \rightarrow \gamma \pi^+ \pi^-$. Thus only the systematic error caused by the MDC tracking from the leptonic pairs need be considered. As the momenta of the two charged leptons are quite low, it is difficult to select a pure sample from data. In this analysis the MDC tracking uncertainty of charged pions at low momentum is determined and used to estimate that of the leptons by reweighting in accordance with their momenta. The data sample of $J/\psi \rightarrow \gamma \eta'$, $\eta' \rightarrow \gamma \pi^+ \pi^-$ is used to evaluate the data-MC difference of pions at low momentum and finally the MDC tracking uncertainty is estimated to be 2.1% for electrons and 1.6% for muons, where the dominant contribution is from the momentum region below 200 MeV/c. Therefore 4.2% and 3.2% are taken as the systematic errors on the tracking efficiency for the channels with $e^+ e^-$ and $\mu^+ \mu^-$, respectively, in the final states.
- (iii) Photon detection efficiency. The photon detection efficiency is studied with three independent decay modes, $\psi(2S) \rightarrow \pi^+ \pi^- J/\psi$ ($J/\psi \rightarrow \rho^0 \pi^0$), $\psi(2S) \rightarrow \pi^+ \pi^- J/\psi$ ($J/\psi \rightarrow l^+ l^-$) and $J/\psi \rightarrow \rho^0 \pi^0$ [23]. The results indicate that the difference between the detection efficiency of data and MC simulation is within 1% for each photon. Since the uncertainty from the radiative photons cancel by measuring the relative branching fraction of $\eta' \rightarrow \pi^+ \pi^- l^+ l^-$ and $\eta' \rightarrow \gamma \pi^+ \pi^-$, 1% is taken to be the systematic error from the photon in η' decaying into $\gamma \pi^+ \pi^-$.

TABLE II. Impact (in %) of the systematic uncertainties on the measured ratios of the branching fractions.

Sources	$\eta' \rightarrow \pi^+ \pi^- e^+ e^-$	$\eta' \rightarrow \pi^+ \pi^- \mu^+ \mu^-$
Form factor uncertainty	0.2	0.3
MDC tracking	4.2	3.2
Photon detection	1.0	1.0
PID	4.0	4.0
4C kinematic fit	2.0	2.0
Background uncertainty	0.9	–
η' mass window	0.1	–
$N_{\eta' \rightarrow \gamma \pi^+ \pi^-}$	0.5	0.5
MC statistics	0.5	0.4
Total	6.3	5.6

- (iv) Particle ID. The study of the particle ID efficiency of the pion is performed using the clean control sample of $J/\psi \rightarrow \pi^+ \pi^- \pi^0$, and indicates that the pion particle ID efficiency for data agrees within 1% of that of the MC simulation in the pion momentum region. The particle ID efficiency of the electron was checked with radiative Bhabha events, and the difference between data and MC simulation is found to be 1%. In this analysis, 4% is taken as the systematic error from the particle ID efficiency of the four charged tracks in η' decaying into $\pi^+ \pi^- l^+ l^-$.
- (v) Kinematic fit. The clean sample $J/\psi \rightarrow \phi \eta$ ($\phi \rightarrow K^+ K^-$, $\eta \rightarrow \pi^+ \pi^- \pi^0$) selected without a kinematic fit is used to estimate the systematic error associated with the 4C kinematic fit. The difference between data and MC is determined to be $(0.47 \pm 1.45)\%$, with $\chi^2 < 75$. In this paper, 1.9% is taken to be the systematic error from the kinematic fit for the analyzed decays of $J/\psi \rightarrow \gamma \eta'$ ($\eta' \rightarrow \pi^+ \pi^- l^+ l^-$). For $J/\psi \rightarrow \gamma \eta'$, $\eta' \rightarrow \gamma \pi^+ \pi^-$ channel, the 4C kinematic fit uncertainty is estimated to be less than 0.7% using the control sample $J/\psi \rightarrow \rho \pi$. Thus, the error from kinematic fit is, 2.0%, the sum of them added in quadrature.
- (vi) Background uncertainty. Studies have shown that the mass resolution of $\gamma \pi^+ \pi^-$, as simulated by the MC, is underestimated. To evaluate the systematic effect associated with this, the invariant mass of $\gamma \pi^+ \pi^-$ in the MC sample is smeared with a Gaussian function, where the width of this Gaussian is floated in the fit. The change of the result, 0.9%, is assigned to be the systematic error.
- (vii) η' mass window requirement. Due to the difference in the mass resolution between data and MC simulation, another source of systematic uncertainty is from the requirement on the η' mass window selection $|M(\pi^+ \pi^- e^+ e^-) - m(\eta')| < 0.02 \text{ GeV}/c^2$. To account for this effect, we examined the detection efficiency by smearing the MC signal shape with a Gaussian function ($\sigma = 0.0022 \pm 0.0012 \text{ GeV}/c^2$), which is obtained from the fit to $M(\pi^+ \pi^- e^+ e^-)$ as we did for the fit of $M(\gamma \pi^+ \pi^-)$. The change of the detection efficiency, 0.1% is assigned for this item.
- (viii) Uncertainty of the number of $\eta' \rightarrow \gamma \pi^+ \pi^-$ events ($N_{\eta' \rightarrow \gamma \pi^+ \pi^-}$). The uncertainty from this item, 0.5%, contains the error due to the π^0 veto cut ($M(\gamma \gamma) > 0.16 \text{ GeV}/c^2$) and the fit-related error.

Except for the systematic uncertainties studied above, a small uncertainty due to the statistical error of the efficiencies in $\eta' \rightarrow \pi^+ \pi^- l^+ l^-$ and $\eta' \rightarrow \gamma \pi^+ \pi^-$ is also considered; all errors are summarized in Table II. The total systematic error is the sum of them added in quadrature.

V. RESULTS

The ratio (upper limit) of $\mathcal{B}(\eta' \rightarrow \pi^+ \pi^- l^+ l^-)$ to $\mathcal{B}(\eta' \rightarrow \gamma \pi^+ \pi^-)$ is calculated with

$$\frac{\mathcal{B}(\eta' \rightarrow \pi^+ \pi^- l^+ l^-)}{\mathcal{B}(\eta' \rightarrow \gamma \pi^+ \pi^-)} = \frac{N_{\eta' \rightarrow \pi^+ \pi^- l^+ l^-} / \epsilon_{\eta' \rightarrow \pi^+ \pi^- l^+ l^-}}{N_{\eta' \rightarrow \gamma \pi^+ \pi^-} / \epsilon_{\eta' \rightarrow \gamma \pi^+ \pi^-}},$$

where $N_{\eta' \rightarrow \pi^+ \pi^- l^+ l^-}$ and $N_{\eta' \rightarrow \gamma \pi^+ \pi^-}$ are the observed events (or the 90% C.L. upper limit) of $\eta' \rightarrow \pi^+ \pi^- l^+ l^-$ and $\eta' \rightarrow \gamma \pi^+ \pi^-$, and $\epsilon_{\eta' \rightarrow \pi^+ \pi^- l^+ l^-}$ and $\epsilon_{\eta' \rightarrow \gamma \pi^+ \pi^-}$ are the corresponding detection efficiencies. With the numbers given in Table I, the ratio $\frac{\mathcal{B}(\eta' \rightarrow \pi^+ \pi^- e^+ e^-)}{\mathcal{B}(\eta' \rightarrow \gamma \pi^+ \pi^-)}$ is determined to be $(7.2 \pm 0.4(\text{stat}) \pm 0.5(\text{syst})) \times 10^{-3}$, where the first error is the statistical error from $N_{\eta' \rightarrow \pi^+ \pi^- l^+ l^-}$ and $N_{\eta' \rightarrow \gamma \pi^+ \pi^-}$. To calculate the upper limit, the systematic error is taken into account by a factor of $\frac{1}{1-\delta_{\text{syst}}}$. Therefore the upper limit, 1.0×10^{-4} , on the ratio $\frac{\mathcal{B}(\eta' \rightarrow \pi^+ \pi^- \mu^+ \mu^-)}{\mathcal{B}(\eta' \rightarrow \gamma \pi^+ \pi^-)}$ is given at the 90% confidence level.

VI. SUMMARY

The measurements of $\eta' \rightarrow \pi^+ \pi^- l^+ l^-$, $l^\pm = (e^\pm, \mu^\pm)$ are performed using the sample of 225.3 million J/ψ events collected with the BESIII detector. A clear signal is observed in the invariant mass spectrum of $\pi^+ \pi^- e^+ e^-$, and the ratio $\frac{\mathcal{B}(\eta' \rightarrow \pi^+ \pi^- e^+ e^-)}{\mathcal{B}(\eta' \rightarrow \gamma \pi^+ \pi^-)}$ is determined to be $(7.2 \pm 0.4(\text{stat}) \pm 0.5(\text{syst})) \times 10^{-3}$. Using the PDG world average of $\mathcal{B}(\eta' \rightarrow \gamma \pi^+ \pi^-)$ and its uncertainty [3], the branching fraction is measured to be $\mathcal{B}(\eta' \rightarrow \pi^+ \pi^- e^+ e^-) = (2.11 \pm 0.12(\text{stat}) \pm 0.14(\text{syst})) \times 10^{-3}$ which is consistent with the theoretical predictions and previous measurement, but with the precision improved significantly. The mass spectra of $\pi^+ \pi^-$ and $e^+ e^-$ are also consistent with the theoretical predictions that $M_{\pi^+ \pi^-}$ is dominated by ρ^0 , and $M_{e^+ e^-}$ has a peak just above $2m_e$

with a long tail. No evidence for η' decaying into $\pi^+ \pi^- \mu^+ \mu^-$ is found, and an upper limit of 1.0×10^{-4} on the ratio of $\frac{\mathcal{B}(\eta' \rightarrow \pi^+ \pi^- \mu^+ \mu^-)}{\mathcal{B}(\eta' \rightarrow \gamma \pi^+ \pi^-)}$ is obtained at the 90% confidence level. The corresponding branching fraction upper limit of $\eta' \rightarrow \pi^+ \pi^- \mu^+ \mu^-$ is $\mathcal{B}(\eta' \rightarrow \pi^+ \pi^- \mu^+ \mu^-) < 2.9 \times 10^{-5}$.

ACKNOWLEDGMENTS

The BESIII collaboration thanks the staff of BEPCII and the computing center for their hard efforts. This work is supported in part by the Ministry of Science and Technology of China under Contract No. 2009CB825200; National Natural Science Foundation of China (NSFC) under Contracts No. 10625524, No. 10821063, No. 10825524, No. 10835001, No. 10935007, No. 10979033, No. 10979012, No. 11105101, No. 11125525, No. 11175189, and No. 11235011; Joint Funds of the National Natural Science Foundation of China under Contracts No. 11079008, and No. 11179007; the Chinese Academy of Sciences (CAS) Large-Scale Scientific Facility Program; CAS under Contracts No. KJCX2-YW-N29, and No. KJCX2-YW-N45; 100 Talents Program of CAS; German Research Foundation DFG under Contract No. Collaborative Research Center CRC-1044; Istituto Nazionale di Fisica Nucleare, Italy; Ministry of Development of Turkey under Contract No. DPT2006K-120470; U.S. Department of Energy under Contracts No. DE-FG02-04ER41291, No. DE-FG02-05ER41374, and No. DE-FG02-94ER40823; U.S. National Science Foundation; University of Groningen (RuG) and the Helmholtzzentrum fuer Schwerionenforschung GmbH (GSI), Darmstadt; WCU Program of National Research Foundation of Korea under Contract No. R32-2008-000-10155-0. This paper is also supported by the Natural Science Foundation of Shandong Province, China under Contracts No. 2009ZRB02465.

-
- [1] G. R. Kalbfleisch *et al.*, *Phys. Rev. Lett.* **12**, 527 (1964).
 - [2] M. Goldberg *et al.*, *Phys. Rev. Lett.* **12**, 546 (1964).
 - [3] J. Beringer *et al.* (Particle Data Group), *Phys. Rev. D* **86**, 010001 (2012).
 - [4] P. Naik *et al.* (CLEO Collaboration), *Phys. Rev. Lett.* **102**, 061801 (2009).
 - [5] A. Faessler, C. Fuchs, and M. I. Krivoruchenko, *Phys. Rev. C* **61**, 035206 (2000).
 - [6] B. Borasoy and R. Nissler, *Eur. Phys. J. A* **33**, 95 (2007).
 - [7] T. Petri, [arXiv:1010.2378](https://arxiv.org/abs/1010.2378).
 - [8] M. Ablikim *et al.* (BESIII Collaboration), *Chinese Phys. C* **36**, 915 (2012).
 - [9] M. Ablikim *et al.* (BESIII Collaboration), *Nucl. Instrum. Methods Phys. Res., Sect. A* **614**, 345 (2010).
 - [10] S. Agostinelli *et al.*, *Nucl. Instrum. Methods Phys. Res., Sect. A* **506**, 250 (2003).
 - [11] J. Allison, K. Amako, J. Apostolakis, H. Araujo, P. Dubois *et al.*, *IEEE Trans. Nucl. Sci.* **53**, 270 (2006).
 - [12] S. Jadach, B. Ward, and Z. Was, *Comput. Phys. Commun.* **130**, 260 (2000).
 - [13] S. Jadach, B. F. L. Ward, and Z. Was, *Phys. Rev. D* **63**, 113009 (2001).
 - [14] R. G. Ping, *Chinese Phys. C* **32**, 243 (2008).
 - [15] D. J. Lange, *Nucl. Instrum. Methods Phys. Res., Sect. A* **462**, 152 (2001).
 - [16] J. C. Chen, G. S. Huang, X. R. Qi, D. H. Zhang, and Y. S. Zhu, *Phys. Rev. D* **62**, 034003 (2000).

- [17] Z. Y. Zhang, L. Q. Qin, and S. S. Fang, *Chinese Phys. C* **36**, 926 (2012).
- [18] $\frac{d\Gamma}{dm} \propto k_\gamma^3 q_\pi^3(m) |\text{BW}_\rho^{\text{GS}}(1 + \delta \frac{m^2}{m_\rho^2} \text{BW}_\omega) + \beta|^2$, where k_γ is the photon energy and $q_\pi(m)$ is the momentum of pion in the $\pi^+\pi^-$ rest frame. BW_ω represents a simple Breit-Wigner function for ω , $\text{BW}_\rho^{\text{GS}}$ is the Breit-Wigner distribution in GS parametrization [19]. $|\delta|$ represents the contribution from ω resonance and the complex phase of δ represents the interference between ω and $\rho(770)$ resonance. m_ρ is the mass of the $\rho(770)$ resonance. β is the constant ratio, which represents the nonresonant contribution.
- [19] G. J. Gounaris and J. J. Sakurai, *Phys. Rev. Lett.* **21**, 244 (1968).
- [20] A. Abele *et al.* (Crystal Barrel Collaboration), *Phys. Lett. B* **402**, 195 (1997).
- [21] R. R. Akhmetshin *et al.* (CMD-2 Collaboration), *Phys. Lett. B* **527**, 161 (2002).
- [22] M. Benayoun, M. Feindt, M. Girone, A. Kirk, Ph. Leruste, J.-L. Narjoux, and K. Šafařík, *Z. Phys. C* **58**, 31 (1993).
- [23] M. Ablikim *et al.* (BESIII Collaboration), *Phys. Rev. D* **83**, 112005 (2011).